*IOSR Journal of Mathematics (IOSR-JM)*
*e-ISSN: 2278-0661, p-ISSN: 2278-8727, Volume 21, Issue 6, Ser. 3 (Nov. – Dec. 2025), PP 22-31*
*www.iosrjournals.org*

# MHD Maxwell Nano Fluid Flow With Double-Diffusive Effects And Chemical Reaction Over A Stretching Surface In A Porous Medium

P. Rameshbabu And Srinivasa Raju
*Department Of Mathematics, Guru Nanak Institute Of Technology, Khanapur, Ibrahimpatnam, Hydearbad 501506 Telangana, India.*
*Department Of Mathematics, Gitams University, Hydearbad Telangana, India.*

***Abstract:***
*The purpose of this research is to investigate the slip flow characteristics of a non-Newtonian Maxwell nanofluid induced by a stretching sheet embedded in a porous medium, under the combined influences of magnetic and chemical processes. The energy equation incorporates the effects of thermophoresis and Brownian motion to capture nanoparticle transport mechanisms. By applying similarity transformations, the governing partial differential equations are reduced to a system of dimensionless ordinary differential equations. These equations are then solved numerically using the Runge–Kutta method in conjunction with the shooting technique.*
*The main objectives of this study are to examine the influence of key physical parameters on the velocity, temperature, and concentration fields and to illustrate these effects through graphical representations. Further, the skin-friction coefficient, Nusselt number, and Sherwood number are computed and presented in tabular form. The numerical results show excellent agreement with previously published benchmark solutions for special cases, confirming the accuracy and reliability of the present analysis.*
***Keywords:*** *Nanofluid; MHD; Maxwell fluid; Porous medium; Chemical reaction; Double diffusion; Stretching sheet;*

---

Date of Submission: 05-12-2025 Date of Acceptance: 15-12-2025

---

## I. Introduction:

The Soret effect is associated with mass flux induced by heat diffusion, whereas the Dufour effect is associated with energy flow caused by solute difference. When dealing with gas concentrations with lighter and medium molecular weights, the Soret impact is used. Many industrial and engineering applications use the Soret and Dufour phenomena to transfer heat and mass, such as multi-component melts in geosciences, groundwater pollutant migration, solidification of binary alloys, chemical reactors, space cooling, isotope separation, oil reservoirs, and gas mixtures. [1]. Bekezhanova and Goncharova [2] examined how the combined acts of Dufour and Soret impacted the characteristics of an evaporating fluid flow. Jawad et al. [3] MHD on the boundary layer was investigated. The Soret, Dufour, and effects were linked to the Marangoni convection via the Darcy-Forchheimer radiative nanofluid flow. investigated the fluid dynamics of spinning disc Soret-Dufour collisions in both uphill and downhill orientations. Shehzad et al. [4]. According to research, the Maxwell's boundary layer contains the components for heat transfer, chemical reaction, and ferrofluid motion by Majeed et al. [5], which also looked at the impacts of Soret and suction. Reddy and Chamkha [6] The impacts of Soret and Dufour on unsteady MHD heat and mass transfer from a permeable stretched sheet with thermophoresis and non-uniform heat generation/absorption were explore [7] used the finite difference method to investigate the Dufour and Soret effects as well as the influence of viscous fluid on the increase in entropy. Siva Reddy Sheri and R. Srinivasa Raju investigated the Soret effect in the presence of viscous dissipation in unsteady MHD free convective flow on a semi-infinite vertical plate. [8]. Anand Rao et al. [9] The finite element approach was used to investigate the unsteady MHD free convection flow across an infinite vertical plate with Soret, Dufour, thermal radiation, and a heat source. Okuyade and co. Shateyi and Motsa [10] applied the successive linearization strategy on partial slip, thermal diffusion, and diffusion-thermo effects for steady MHD convective flow brought on by a spinning disc. Sardar et al. [11] A wedge-shaped mixed convection Carreau nanofluid flow was explored in the presence of Soret and Dufour effects. Ahmad et al [12] found the numerical resolution of four homogeneous parabolic partial differential equations using the non-polynomial cubic spline approach. By using the finite element approach, Ali et al. [13] evaluated the effects of Dufour and Soret impacts on MHD rotational flow of Oldroyd-B nanofluid over a stretched sheet with double diffusion Cattaneo-Christov heat flux

model. Srinivasacharya et al. [14] examined the impact of Soret and Dufour on mixed convection on a vertical wavy surface in a porous medium with a range of characteristics.. Pal and Mondal [15] investigated the effects of thermophoresis and Soret-Dufour on the transfer of heat and mass through a non-isothermal wedge with thermal radiation and Ohmic dissipation. Makinde [16] examined the impact of Soret and Dufour on MHD mixed convection flow using a vertical plate immersed in a porous plate medium. When radiative heat transmission and an irreversible chemical process of the $n^{th}$ order are present, Makinde and Olanrewaju[17] explored the unstable mixed convection of the flow through a binary mixture. It is believed that the fluid is optically thin. The contributions made by Soret and Dufour to numerous academic subjects were examined in several of the research projects ([18]-[23]).

The major objective of this inquiry is to evaluate the interaction between thermal diffusion and diffusion thermo to influence the flow of MHD boundary layer Maxwell fluid through a stretched sheet in the presence of a porous medium containing nanofluid particles. The cornerstone of our inquiry is laid forth in the aforementioned reference documents. The basic governing equations for this inquiry were solved using the Runge-Kutta method and the gunshot method. The Maxwell fluid parameter ($\beta$), the Dufour number ($Du$), the Soret number ($Sr$), the Prandtl number ($Pr$), the Thermophoresis parameter ($Nt$), the Permeability parameter ($K$), the Brownian motion parameter ($Nb$), the Schmidt number ($Sc$), the Chemical reaction parameter ($Kr$), and the Magnetic parameter will all be graphically illustrated in this study to show how they affect concentration, temperature, and velocity profiles ($M$). The Skin-friction, The numerical values of the Nusselt and Sherwood numbers are also given and explained in tabular form. The following is the structure of this work: Section 2 describes the non-linear coupled ordinary differential equations that govern the system. Section 3 discusses the development of the Runge-Kutta technique and a shooting method for solving the governing equations in considerable detail. Section 4 goes into considerable depth concerning the program's code checking. The findings and observations are presented in Section 5. Section 6 goes into further depth about the results.

## II. Flow Governing Equations

The influence of thermal diffusion (Soret effect) and diffusion-thermo (Dufour effect) on a two-dimensional, viscous, steady, incompressible, electrically conducting Maxwell fluid flow over a stretching sheet is examined in this section. The analysis incorporates the effects of an applied magnetic field, a first-order chemical reaction, and flow through a porous medium, together with nanoparticle transport mechanisms governed by Brownian motion and thermophoresis. The physical configuration of the flow is illustrated in Figure 1. The following assumptions are adopted for this investigation: As shown in Fig. 1, the coordinate axes are selected to be the x-axis parallel to the flow direction and the y-axis normal to it.

i. With a velocity of Uw = axe and a stretching value of > 0, the plate is stretched along the x-axis.
ii. The boundary layer occurs if the stretching surface's normal coordinate is provided when $y \geq 0$.
iii. In addition, the effects of Brownian motion and thermophoresis on chemical reactions are taken into account.
iv. Temperature at surface with $T_w$ and far away the surface as $T_\infty$ are symbolized. For concentration the symbols are $C_w$ and $C_\infty$ respectively.
v. The steady and convective Maxwell-nanofluid flow with the boundary layer in the existence of the uniform magnetic field of strength $B_o$.
vi. Since the magnetic Reynolds number is believed to be low, the induced magnetic field can be regarded as insignificant.
vii. In addition, the aforementioned hypotheses permit the ignoring of body forces, viscous dissipation, and Joule heating.

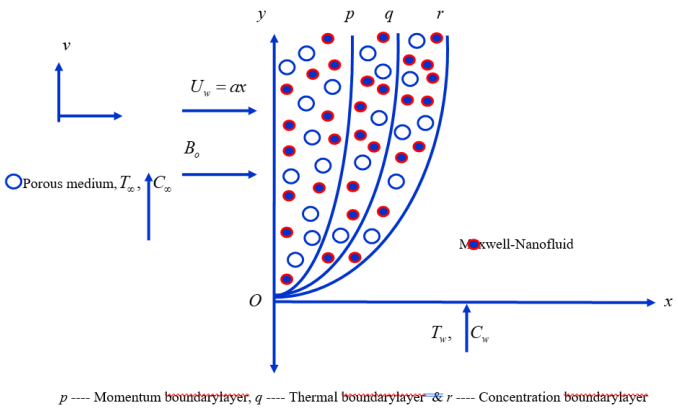


**Fig. 1.:** Geometry representation of the fluid

The fundamental equations regulating stable, two-dimensional, electrically conducting, incompressible Maxwell-nanofluid flow are as follows, based on the foregoing hypotheses:*Continuity Equation:*

$$\frac{\partial u}{\partial x}+\frac{\partial v}{\partial y}=0, \tag{1}$$

*Momentum Equation:*

$$u\frac{\partial u}{\partial x}+v\frac{\partial u}{\partial y}=\nu\frac{\partial^2 u}{\partial y^2}-\beta_1\left(u^2\frac{\partial^2 u}{\partial x^2}+2uv\frac{\partial^2 u}{\partial x\partial y}+v^2\frac{\partial^2 u}{\partial y^2}\right)-\frac{\sigma B_o^2}{\rho}\left(u+\beta_1 v\frac{\partial u}{\partial y}\right)-\nu\left(\frac{u}{k_1}\right), \tag{2}$$

*Equation of thermal energy:*

$$u\frac{\partial T}{\partial x}+v\frac{\partial T}{\partial y}=\alpha_m\frac{\partial^2 T}{\partial y^2}+\tau_B\left\{D_B\frac{\partial C}{\partial y}\frac{\partial T}{\partial y}+\frac{D_T}{T_\infty}\left(\frac{\partial T}{\partial y}\right)^2\right\}+\frac{D_m K_T}{C_s C_p}\left(\frac{\partial^2 C}{\partial y^2}\right), \tag{3}$$

*Equation of species nanoparticle volume concentration:*

$$u\frac{\partial C}{\partial x}+v\frac{\partial C}{\partial y}=D_B\frac{\partial^2 C}{\partial y^2}+\frac{D_T}{T_\infty}\frac{\partial^2 T}{\partial y^2}-k_r\left(C-C_\infty\right)+\frac{D_m K_T}{T_m}\left(\frac{\partial^2 T}{\partial y^2}\right), \tag{4}$$

For this flow The boundary conditions are

$$\left.\begin{aligned} &u=U_w(x)=ax,\ T=T_w,\ C=C_w\ \ at\ \ y=0\\ &u\to 0,\ T\to T_\infty,\ C\to C_\infty\ \ as\ \ y\to\infty \end{aligned}\right\} \tag{5}$$

The following similarity transformation can be used to convert the governing equations into ordinary differential equations.

$$\left.u=axf'(\eta),\ v=-\sqrt{a\nu}\,f(\eta),\ \eta=y\sqrt{\frac{a}{\nu}},\ \ \theta=\frac{T-T_\infty}{T_w-T_\infty},\ \phi=\frac{C-C_\infty}{C_w-C_\infty}\right\}, \tag{6}$$

The essential governing equations (2), (3), and (4), as well as boundary conditions (5), have the following forms using the similarity transformations (6)

$$f'''+ff''-\left(f'^2\right)+\beta\left(2ff'f''-f^2f'''\right)-\left(M+K\right)f'+M\beta f\,f''=0, \tag{7}$$

$$\theta''+\Pr f\theta'+\Pr Nb\theta'\phi'+\Pr Nt\theta'^2+\Pr Du\phi''=0, \tag{8}$$

$$Nb\phi''+NbScf\phi'+Nt\theta''-ScKr\phi+ScSrNb\theta''=0, \tag{9}$$

the corresponding boundary conditions (5) become

$$\left.f'(0)=1,\ f(0)=0,\ \theta(0)=1,\ \phi(0)=1,\ f'(\infty)\to 0,\ \theta(\infty)\to 0,\ \phi(\infty)\to 0\right\}, \tag{10}$$

where the involved physical parameters are defined as

$$\left.\begin{aligned} &M=\frac{\sigma B_o^2}{\rho a},\ K=\frac{\nu}{ak_1},\ \Pr=\frac{\nu}{\alpha_m},\ Nb=\frac{\tau_B D_B\left(C_w-C_\infty\right)}{\nu},\ \beta=\beta_1 a,\ Kr=\frac{k_r}{a},\\ &Sc=\frac{\nu}{D_B},\ Nt=\frac{\tau_B D_T\left(T_\infty-T_m\right)}{\nu T_\infty},\ Sr=\frac{D_m K_T(T_w-T_\infty)}{T_m\nu\left(C_w-C_\infty\right)},\ Du=\frac{D_m K_T\left(C_w-C_\infty\right)}{C_s C_p\nu\left(T-T_\infty\right)}, \end{aligned}\right\}, \tag{11}$$

The physical quantities of interest like Skin-friction coefficient (*Cf*), local Nusselt number (*Nu*) and local Sherwood number (*Sh*) are defined as

$$C_f=\frac{\tau_w}{\rho U_w^2}=\frac{1}{\rho U_w^2}\mu\left(\frac{\partial u}{\partial y}\right)_{y=0}\Rightarrow Cf=C_f\left(\sqrt{\mathrm{Re}_x}\right)=f''(0) \tag{12}$$

$$Nu_x = \frac{xq_w}{\kappa\left(T_w - T_\infty\right)} = -\frac{x\kappa\left(\dfrac{\partial T}{\partial y}\right)_{y=0}}{\kappa\left(T_w - T_\infty\right)} \Rightarrow Nu = Nu_x\left(\mathrm{Re}_x\right)^{\frac{-1}{2}} = -\theta'(0) \tag{13}$$

$$Sh_x = \frac{xq_m}{D_B\left(C_w - C_\infty\right)} = -\frac{D_B\left(\dfrac{\partial C}{\partial y}\right)_{y=0}}{\left(C_w - C_\infty\right)} \Rightarrow Sh = Sh_x\left(\mathrm{Re}_x\right)^{\frac{-1}{2}} = -\phi'(0) \tag{14}$$

## III. Method of Solution by Runge-Kutta method:

A complete set of Eqs (7)–(9) does not appear to have an accurate solution. This is because the equations in (7) to (9) are nonlinear and Eq. (10) provides sufficient boundary conditions, necessitating the use of numerical techniques to tackle the issue. The controlling partial differential equations are transformed into a set of non-linear ordinary differential equations that may be solved numerically using a similarity transformation. The boundary value problem resulting from this is numerically resolved by combining the shooting method with a fourth-order Runge-Kutta scheme. Decomposing the nonlinear differential equations into a set of first-order differential equations yields a collection of first-order differential equations. The corresponding ordinary differential equations ((7)–(9)) have been condensed to system of seven simultaneous equations for seven unknowns. The coupled ordinary differential Eqs. (7)-(9) are third order in $f(\eta)$ and second order in $\theta(\eta)$ and $\phi(\eta)$ which have been reduced to a system of seven simultaneous equations for seven unknowns. In order to numerically solve this system of equation ns using Runge-Kutta method, the solutions require seven initial conditions but two initial conditions in $f(\eta)$ one initial condition in each of $\theta(\eta)$ and $\phi(\eta)$ are known. However, the values of $f'(\eta)$, $\theta(\eta)$ and $\phi(\eta)$ are known at $\eta \to \infty$. These end conditions are utilized to produce unknown initial conditions at $\eta = 0$ by using shooting technique. The most important step of this scheme is to choose the appropriate finite value of $\eta_\infty$. Thus to estimate the value of $\eta_\infty$ we start with some initial guess value and solve the boundary value problem consisting of Eqs. (7)-(9) to obtain $f''(0)$, $\theta'(0)$ and $\phi'(0)$. The solution process is repeated with another larger value of $\eta_\infty$ until two successive values of $f''(0)$, $\theta'(0)$ and $\phi'(0)$ differ only after desired significant digit. The last value $\eta_\infty$ is taken as the finite value of the limit $\eta_\infty$ for the particular set of physical parameters for determining velocity, temperature and concentration, respectively, are $f(\eta)$, $\theta(\eta)$ and $\phi(\eta)$ in the boundary layer. After getting all the initial conditions we solve this system of simultaneous equations using fourth order Runge-Kutta integration scheme. The value of $\eta_\infty$ is selected to 8 depending on the physical parameters governing the flow so that no numerical oscillation would occur. Thus, the coupled boundary value problem of third-order in $f(\eta)$, second-order in $\theta(\eta)$ and $\phi(\eta)$ has been reduced to a system of seven simultaneous equations of first-order for seven unknowns as follows:

$$\left.\begin{aligned} &f' = p \Rightarrow f'' = p' = q \Rightarrow f''' = p'' = q' \Rightarrow q' = \frac{Mp + Kp + p^2 - fq - 2\beta fpq - M\beta fq}{\left(1 - \beta f^2\right)} \\ &\theta' = r \Rightarrow \theta'' = r' \text{ then } r' = -\left(\mathrm{Pr}\right)fr - \left(\mathrm{Pr}\right)\left(Nb\right)rz - \left(\mathrm{Pr}\right)\left(Nt\right)r^2 - \left(\mathrm{Pr}\right)\left(Du\right)z' \\ &\& \\ &\phi' = z \Rightarrow \phi'' = z' \text{ then } Nbz' = -\left(Sc\right)\left(Nb\right)fz - \left(Nt\right)r' + \left(Sc\right)\left(Kr\right)\phi - \left(Sc\right)\left(Sr\right)\left(Nb\right)r' \end{aligned}\right\} \tag{15}$$

and the corresponding boundary conditions became

$$p(0) = 1,\ f(0) = 0,\ \theta(0) = 1,\ \phi(0) = 1,\ p(\infty) \to 0,\ \theta(\infty) \to 0,\ \phi(\infty) \to 0 \tag{16}$$

The initial value problem (IVP), which is then further investigated, is first transformed from the boundary value issue. The shooting approach is then used to repeatedly solve the beginning value problem by correctly estimating the missing starting value for different combinations of components. In this case, the step size for calculations is set at h = 0.1. Furthermore, a 10-6 error tolerance is applied. Tables and graphs are used to illustrate the material, which includes an in-depth examination of the problems' key characteristics.

## IV. Program Code Validation:

**Table-1.:** Comparison of current rate of heat transfer (Nusselt number) coefficient results with published results of Makinde and Aziz [36] when $M = \beta = Nb = Nt = K = Kr = Sr = Du = 0$

| Pr | Nusselt number results of Makinde and Aziz [23] | Present Nusselt number results |
|---|---|---|
| 0.200 | 0.1691 | 0.156783193846394834386938 4 |
| 0.700 | 0.4539 | 0.440901098769038679857985 1 |
| 7.000 | 1.8954 | 1.888577513737638763087638 7 |
| 20.00 | 3.3539 | 3.345677684837963100736765 3 |
| 70.00 | 6.4622 | 6.457881048419837645986496 2 |

From table-1, the authors have discussed the comparison of present results with published analytical results of Makinde and Aziz [23] for program code validation in absence of Magnetic field, Maxwell fluid, Porous medium, Thermophoresis, Brownian motion, Soret number, Chemical reaction and Dufour number effects. In this table, the present results are very good agreement and coincide with the published results.

## V. Results and Discussion:

In this section, the obtained numerical solutions of velocity, temperature and concentration profiles are discussed using graphs for variations of different physical parameters such as Magnetic field parameter ($M$ = 0.1, 0.3, 0.5, 0.8), Permeability parameter ($K$ = 0.3, 0.5, 0.7, 1.0), Maxwell fluid parameter ($\beta$ = 0.2, 0.4, 0.6, 1.0), Prandtl number (Pr = 0.71, 1.0, 3.0, 7.0), Thermophoresis parameter ($Nt$ = 0.1, 0.3, 0.5, 0.7), Brownian motion parameter ($Nb$ = 0.1, 0.2, 0.3, 0.4), Dufour number ($Du$ = 0.5, 1.0, 1.5, 2.0), Soret number ($Sr$ = 0.5, 1.0, 1.5, 2.0), Chemical reaction parameter ($Kr$ = 0.5, 0.8, 1.2, 1.5) and Schmidt number ($Sc$ = 0.22, 0.30, 0.60, 0.78) in figures 3, 4, 5, 6, 7, 8, 9, 10, 11, 12, 13, 14. Also the numerical values of additional quantities such as Skin-friction coefficient ($Cf$), Rate of heat transfer coefficient in terms of Nusselt number ($Nu$) and Rate of mass transfer coefficient in terms of Sherwood number ($Sh$) are discussed and presented in tabular forms.

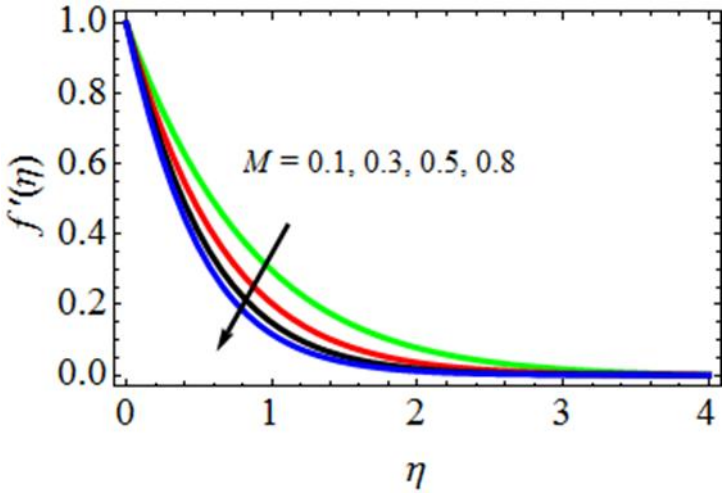


**Fig. 3.** $M$ effect on velocity profiles

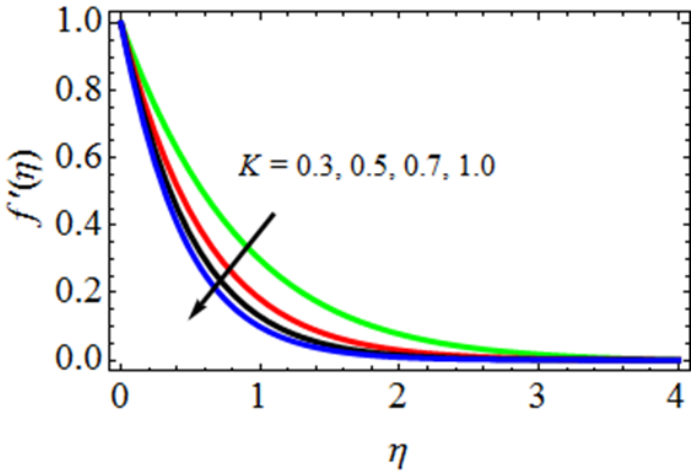


**Fig. 4.** $K$ effect on velocity profiles

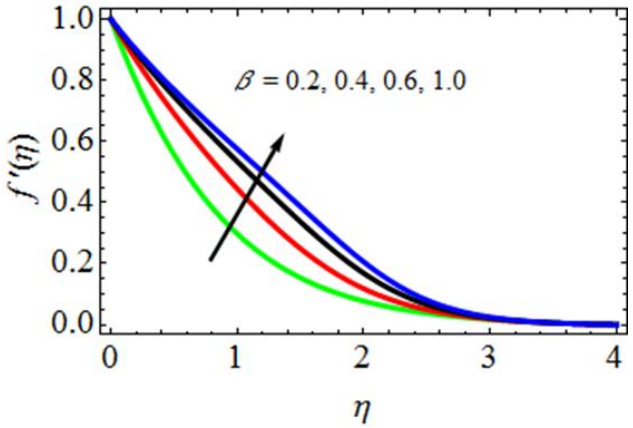


**Fig. 5.** $\beta$ effect on velocity profiles

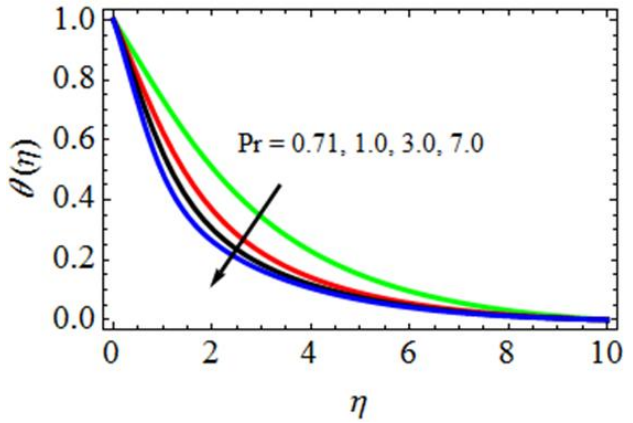


**Fig. 6.** Pr effect on temperature profiles

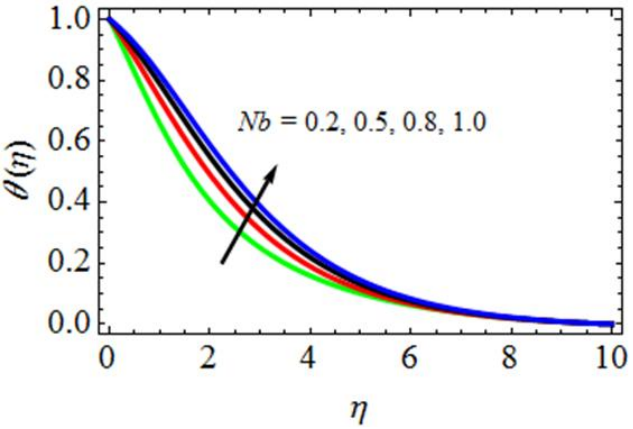


**Fig. 7.** *Nb* effect on temperature profiles

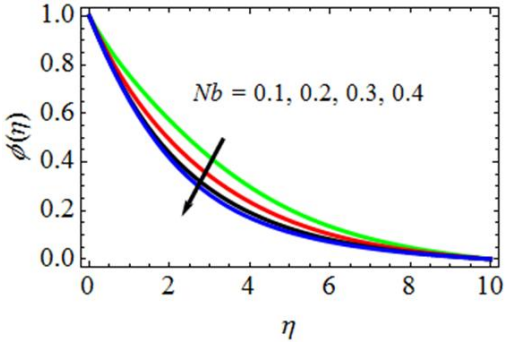


**Fig. 8.** *Nb* effect on concentration profiles

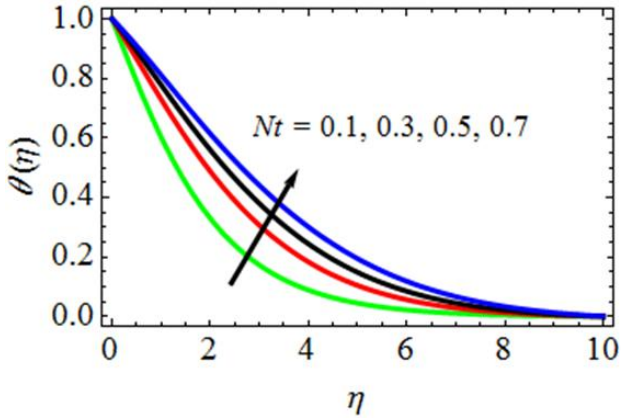


**Fig. 9.** *Nt* effect on temperature profiles

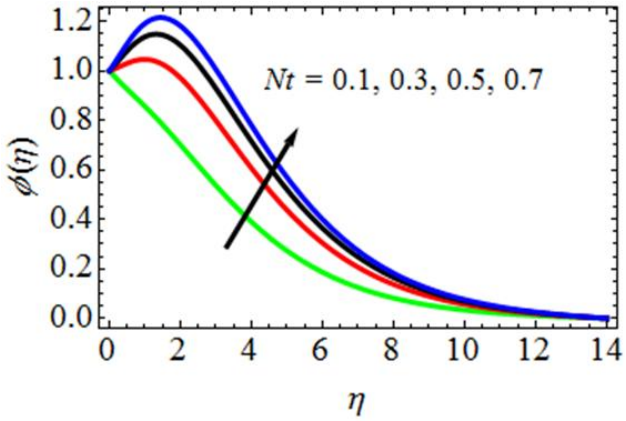


**Fig. 10.** *Nt* effect on concentration profiles

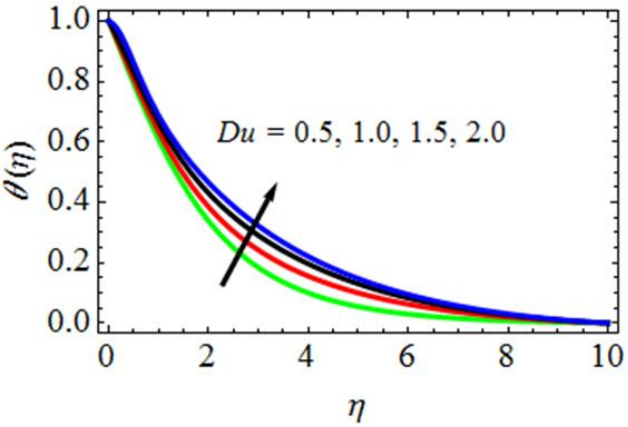


**Fig. 11.** *Du* effect on temperature profiles

Fig. 3 demonstrates the variations of Magnetic field parameter ($M$ = 0.1, 0.3, 0.5, 0.8) on stream wise velocity profiles. It is observed that there is inverse relationship between magnetic parameter and stream wise velocity profiles. This is due to the fact that with increase in magnetic parameter a force is produce, which is notable as Lorentz force. With the production of this force a resistive force induces, in opposite to the motion of fluid particles. Therefore reduction takes place in stream wise velocity. Fig. 4 demonstrates the effect of Permeability parameter ($K$ = 0.3, 0.5, 0.7, 1.0) on velocity profiles. It is obvious that the presence of porous medium causes higher restriction to the fluid flow, which in turn slows its motion. Therefore, with increasing permeability parameter, the resistance to the fluid motion increases and hence velocity decreases. The influence of Maxwell fluid parameter ($\beta$ = 0.2, 0.4, 0.6, 1.0) physical parameters on the non-dimensional velocity profiles is discussed in Fig. 5. From this figure, it is seen that a rise in the parametric values of Maxwell fluid parameter increases the velocity profiles. Fig. 6 illustrates impact of Prandtl Number (Pr = 0.71, 1.0, 3.0, 7.0).

Enhancement in Prandtl number causes decrease in temperature profile. Prandtl parameter is inversely proportional to thermal diffusivity. Higher estimations of Prandtl parameter show lesser thermal diffusivity which causes a decline in temperature distribution. Increase in the Prandtl number tend to decrease the thermal diffusivity which slows down diffusion of temperature and hence the thermal sketch is decreased. The effect of the Brownian motion parameter (*Nb* = 0.1, 0.2, 0.3, 0.4) on temperature and concentration profiles is shown in Figs. 7 and 8 respectively. The temperature profile settled at higher values by an increase in the Brownian motion parameter. Brownian motion is the random motion due to the collisions between nanoparticles and base fluid. More is the Brownian motion parameter; more is the collision. Due to collision between particles, the internal kinetic energy of the fluid increases. There is a reverse relationship between the Brownian motion parameter and concentration profile. More is the Brownian motion parameter; less is the number of nanoparticles in the base fluid. Figs. 9 and 10 reveal the impact of thermophoresis parameter (*Nt* = 0.1, 0.3, 0.5, 0.7) on temperature and concentration profiles. Both temperature and concentration profiles increase for higher values of *Nt*. Thermophoresis is the transport force that occurs due to the temperature gradient between layers of the fluid. More Thermophoresis parameter means that the temperature difference between the layer increases, so the heat transformation rate also increases. By increasing the nanoparticles, the concentration of the fluid increases. More is the nanoparticles more is the heat transformation between the layers, so *Nt* increases both temperature profiles as well as concentration profiles. Fig. 11 portrayed that fluid temperature profile increase with the enlargement in Dufour number (*Du* = 0.5, 1.0, 1.5, 2.0). Physically this phenomenon can be explained as if two different (chemically) non reacting fluids of the same temperature were released to diffuse in the system, then the difference in the temperature of the system increases.

**Table-2.:** Skin-friction coefficient values for variations of *M*, *β*, *K*, *Du*, *Sr*, Pr, *Sc*, *Nb*, *Nt*, *Kr*

| *M* | *β* | *K* | *Du* | *Sr* | Pr | *Sc* | *Nb* | *Nt* | *Kr* | *Cf* |
|---|---|---|---|---|---|---|---|---|---|---|
| 0.1 | 0.2 | 0.3 | 0.5 | 0.5 | 0.71 | 0.22 | 0.1 | 0.1 | 0.5 | 1.866670936130946 |
| **0.3** | | | | | | | | | | 1.824683908634963 |
| **0.5** | | | | | | | | | | 1.804750834601374 |
| | **0.4** | | | | | | | | | 1.838787958719321 |
| | **0.6** | | | | | | | | | 1.793756086107565 |
| | | **0.5** | | | | | | | | 1.841098371349770 |
| | | **0.7** | | | | | | | | 1.829986771383458 |
| | | | **1.0** | | | | | | | 1.880934871346103 |
| | | | **1.5** | | | | | | | 1.906768410971341 |
| | | | | **1.0** | | | | | | 1.872293606407634 |
| | | | | **1.5** | | | | | | 1.896768709873987 |
| | | | | | **1.00** | | | | | 1.823313874513345 |
| | | | | | **3.00** | | | | | 1.797686731093831 |
| | | | | | | **0.30** | | | | 1.832659065109639 |
| | | | | | | **0.60** | | | | 1.800875207687520 |
| | | | | | | | **0.2** | | | 1.885672098673023 |
| | | | | | | | **0.3** | | | 1.896475630746384 |
| | | | | | | | | **0.3** | | 1.893473134444993 |
| | | | | | | | | **0.5** | | 1.906574986498469 |
| | | | | | | | | | **0.8** | 1.840456209794985 |
| | | | | | | | | | **1.2** | 1.826768736173396 |

**Table-3.:** Rate of heat transfer coefficient (Nusselt number) values for variations of Pr, *Du*, *Nb*, *Nt*

| Pr | *Du* | *Nb* | *Nt* | *Nu* |
|---|---|---|---|---|
| 0.71 | 0.5 | 0.1 | 0.1 | 0.686916397613946 |
| **1.00** | | | | 0.656398619306109 |
| **3.00** | | | | 0.616874619346331 |
| | **1.0** | | | 0.706787193843716 |
| | **1.5** | | | 0.726786734673461 |
| | | **0.2** | | 0.696768567298407 |
| | | **0.3** | | 0.706785296736903 |
| | | | **0.3** | 0.716786798678676 |
| | | | **0.5** | 0.729875765429429 |

**Table-4.:** Rate of mass transfer coefficient (Sherwood number) values for variations of *Sc*, *Sr*, *Nb*, *Nt*, *Kr*

| *Sc* | *Sr* | *Nb* | *Nt* | *Kr* | *Sh* |
|---|---|---|---|---|---|
| 0.22 | 0.5 | 0.1 | 0.1 | 0.5 | 1.246787390873694 |
| **0.30** | | | | | 1.218678179879863 |
| **0.60** | | | | | 1.181374308530672 |
| | **1.0** | | | | 1.266768769876958 |
| | **1.5** | | | | 1.286758672986742 |
| | | **0.2** | | | 1.220982987498628 |

| | | | | | |
|---|---|---|---|---|---|
| | | **0.3** | | | 1.205667096190669 |
| | | | **0.3** | | 1.266798679681791 |
| | | | **0.5** | | 1.286798579856713 |
| | | | | **0.8** | 1.226786578964793 |
| | | | | **1.2** | 1.206786798673982 |

## VI. Conclusions:

The effects of thermophoresis, thermal diffusion (Soret and Dufour), Brownian motion, and electrical conductivity on a two-dimensional, steady, incompressible, viscous, Maxwell fluid flow towards a stretching sheet in the presence of nanofluid particles, porous medium, magnetic field, and chemical reaction model are investigated in the current research work. For this inquiry, the Runge-Kutta method and the shot approach are used to solve the resulting governing flow equations. The aspire of this research article is to examine the impacts of $M$, $\beta$, $K$, $Du$, $Sr$, Pr, $Sc$, $Nb$, $Nt$, $Kr$. Graphical and tabular studies are done on flow variables including velocity, temperature, and concentration profiles as well as skin friction, rate of heat transfer, and mass transfer coefficients. The primary conclusions of this inquiry are:

- ✓ Decreasing the temperature field due to rising the values of the Prandtl number and the opposite effect is noticed in case of Thermophoresis, Dufour number and Brownian motion parameters.
- ✓ By increasing in Schmidt number, Chemical reaction, Brownian motion parameters the concentration profiles is reduced and increased in case of Thermophoresis and Soret parameters.
- ✓ Finally, the obtained numerical results are more accurated with the published results of Makinde and Aziz [23] in a limiting case by taking $M \to 0$, $\beta \to 0$, $Nb \to 0$, $Nt \to 0$, $K \to 0$, $Kr \to 0$, $Sr \to 0$, and $Du \to 0$.

## References:


[1]. Bekezhanova, V. B., Goncharova O. N., Influence Of The Dufour And Soret Effects On The Characteristics Of Evaporating Liquid Flows. Int. J. Heat Mass Tran. 2020; 154: 119696.

[2]. Salleh SNA, Bachok N, Arifin NM, Ali FM. Influence Of Soret And Dufour On Forced Convection Flow Towards A Moving Thin Needle Considering Buongiorno's Nanofluid Model. Alex Eng. J. 2020;59(5):3897-3906. Doi: 10.1016/J.Aej.2020.06.045.

[3]. A. Majeed, A. Zeeshan, R. Ellahi, Chemical Reaction And Heat Transfer On Boundary Layer Maxwell Ferro-Fluid Flow Under Magnetic Dipole With Soret And Suction Effects, Eng. Sci. Technol., 20 (3) (2017), Pp. 1122-1128.

[4]. A. A. Yinusa, M. G. Sobamowo, M. A. Usman, E. H. Abubakar, Exploration Of Three Dimensional Squeezed Flow And Heat Transfer Through A Rotating Channel With Coupled Dufour And Soret Influences, Therm. Sci. Eng. Progr., 21 (2021), Article 100788.

[5]. S. A. Khan, T. Hayat, A. Alsaedi, Irreversibility Analysis In Darcy-Forchheimer Flow Of Viscous Fluid With Dufour And Soret Effects Via Finite Difference Method, Case Stud. Therm. Eng., 26 (2021), T. Hayat, S. Asghar, A. Tanveer, A. Alsaedi, Chemical Reaction In Peristaltic Motion Of MHD Couple Stress Fluid In Channel With Soret And Dufour Effects, Results Phys., 10 (2018), Pp. 69-80.

[6]. J. Anand Rao, P. Ramesh Babu And R. Srinivasa Raju, Finite Element Analysis Of Unsteady MHD Free Convection Flow Past An Infinite Vertical Plate With Soret, Dufour, Thermal Radiation And Heat Source, ARPN Journal Of Engineering And Applied Sciences, Vol. 10, No. 12, Pp. 5338-5351,2015.

[7]. W. I. A. Okuyade, T. M. Abbey, A. T. Gima-Laabel, Unsteady MHD Free Convective Chemically Reacting Fluid Flows Over A Vertical Plate With Thermal Radiation, Dufour, Soret, And Constant Suction Effects, Alex. Eng. J., 57 (2018), Pp. 3863-3871.

[8]. Humara Sardar, Latif Ahmad, Masood Khan, Ali Saleh Alshomrani, Investigation Of Mixed Convection Carreau Nanofluid Flow Over A Wedge In The Presence Of Soret And Dufour Effects, Int. J. Heat Mass Transf., 137 (2019), Pp. 809-822.

[9]. K. Sharada, B. Shankar, Soret And Dufour Effects On MHD Mixed Convection Flow Of Carreau Nanofluid Over An Exponentially Stretching Sheet With Concentration Slip,J. Nanofluids, 6 (6) (2017), Pp. 1143-1148.

[10]. B. Ahmad, A. Perviz, M. O. Ahmad, F. Dayan, Numerical Solution With Non-Polynomial Cubic Spline Technique Of Order Four Homogeneous Parabolic Partial Differential Equations,Sci. Inq. Rev., 5 (4) (2021).

[11]. B. Ali, S. Hussain, Y. Nie, A. K. Hussein, D. Habib, Finite Element Investigation Of Dufour And Soret Impacts On MHD Rotating Flow Of Oldroyd-B Nanofluid Over A Stretching Sheet With Double Diffusion Cattaneochristov Heat Flux Model, Powder Technol., 377 (2021), Pp. 439-452.

[12]. D. Srinivasacharya, B. Mallikarjuna, R. Bhuvanavijaya, Soret And Dufour Effects On Mixed Convection Along A Vertical Wavy Surface In A Porous Medium With Variable Properties, Ain Shams Eng. J., 6 (2) (2015), Pp. 553-564, 10.1016/J.Asej.2014.11.007.

[13]. O. D. Makinde, On MHD Mixed Convection With Soret And Dufour Effects Past A Vertical Plate Embedded In A Porous Plate Medium, Latin Amer Appl Res, 41 (2011), Pp. 63-68.

[14]. O. D. Makinde, O. P. Olanrewaju, Unsteady Mixedconvection With Soret And Dufour Effects Past A Porous Plate Moving Through A Binary Mixture Of Chemically Reacting Fluid, Chem Engcommun, 198 (7) (2011), Pp. 920-938.

[15]. Aly A. M., Natural Convection Over Circular Cylinders In A Porous Enclosure Filled With A Nanofluid Under Thermo-Diffusion Effects, J. Taiwan Inst. Chem. Eng., 70 (2017), Pp. 88-103.

[16]. Arun S., Satheesh A., Mesoscopic Analysis Of MHD Double Diffusive Natural Convection And Entropy Generation In An Enclosure Filled With Liquid Metal, J. Taiwan Inst. Chem. Eng., 95 (2019), Pp. 155-173.

[17]. Chamkha A. J., Al-Naser H., Hydromagnetic Double-Diffusive Convection In A Rectangular Enclosure With Opposing Temperature And Concentration Gradients, Int. J. Heat Mass Transfer, 45 (12) (2002), Pp. 2465-2483.

[18]. J. -T. Hu, S. -J. Mei, Combined Thermal And Moisture Convection And Entropy Generation In An Inclined Rectangular Enclosure Partially Saturated With Porous Wall: Nonlinear Effects With Soret And Dufour Numbers, Int. J. Mech. Sci., 199 (2021), Article 106412.

[19]. Idowu A. S., Falodun B. O., Variable Thermal Conductivity And Viscosity Effects On Non-Newtonian Fluids Flow Through A Vertical Porous Plate Under Soret-Dufour Influence, Math Comput Simulation, 177 (2020), Pp. 358-384.

[20]. Ali A., Sajjad A., Asghar S., Thermal-Diffusion And Diffusion-Thermo Effects In A Nanofluid Flow With Nonuniform Heat Flux And Convective Walls, Journal Of Nanofluids, 8 (6) (2019), Pp. 1367-1372.

[21]. Akolade M. T., Idowu A. S., Adeosun A. T., Multislip And Soret-Dufour Influence On Nonlinear Convection Flow Of MHD Dissipative Casson Fluid Over A Slendering Stretching Sheet With Generalized Heat Flux Phenomenon, Heat Transf Res, 50 (5) (2021), Pp. 3913-3933.
[22]. Layek G., Mandal B., Bhattacharyya K., Dufour And Soret Effects On Unsteady Heat And Mass Transfer For Powell-Eyring Fluid Flow Over An Expanding Permeable Sheet, J Appl Comput Mech, 6 (4) (2020), Pp. 985-998.
[23]. O. D. Makinde, A. Aziz, Boundary Layer Flow Of A Nanofluid Past A Stretching Sheet With A Convective Boundary Condition, Int. J. Therm. Sci. 50 (2011) 1326-1332.